Quantum contributions in the ice phases: The path to a new empirical model for water—TIP4PQ/2005

Carl McBride,[1] Carlos Vega,[1,a)] Eva G. Noya,[1] Rafael Ramírez,[2] and Luis M. Sesé[3]
[1]*Dept. Química-Física I, Fac. de Ciencias Químicas, Universidad Complutense de Madrid, 28040 Madrid, Spain*
[2]*Instituto de Ciencia de Materiales, CSIC, Campus de Cantoblanco, 28049 Madrid, Spain*
[3]*Dept. Ciencias y Técnicas Fisicoquímicas, Fac. de Ciencias, UNED, Paseo Senda del Rey 9, 28040 Madrid, Spain*

(Received 15 April 2009; accepted 19 June 2009; published online 14 July 2009)

With a view to a better understanding of the influence of atomic quantum delocalization effects on the phase behavior of water, path integral simulations have been undertaken for almost all of the known ice phases using the TIP4P/2005 model in conjunction with the rigid rotor propagator proposed by Müser and Berne [Phys. Rev. Lett. **77**, 2638 (1996)]. The quantum contributions then being known, a new empirical model of water is developed (TIP4PQ/2005) which reproduces, to a good degree, a number of the physical properties of the ice phases, for example, densities, structure, and relative stabilities. © *2009 American Institute of Physics*. [DOI: 10.1063/1.3175694]

I. INTRODUCTION

"Water, water, every where…" goes the poet Samuel Taylor Coleridge's *The Rime of the Ancient Mariner*, which provides a magnificent résumé of our reason for studying this ubiquitous material. Many volumes have been written about water and ice (to cite just a few[1–5]), and a good deal more await writing before we fully understand this enigmatic molecule.

Currently the point has been reached where many properties, including the global phase diagram of water and the ice phases, can be reproduced qualitatively (and in some cases, quantitatively) using little more than a simple empirical model.[6] However, there are several aspects of water where our knowledge, and thus our understanding, is far from complete. One such aspect is the high pressure/temperature region of the phase diagram, where the precise location of the melting curves is still yet to be agreed upon due to the difficult nature of the experiments. For example, it is an open question as to whether water becomes superionic in this region.[7,8] In one of the ice polymorphs, ice X, the notion of a water molecule even becomes lost, the protons being shared equally between oxygen atoms.[9,10] The low temperature region of the phase diagram is also extremely interesting, where a host of "anomalous" or atypical trends are also present. Examples are the well known maximum in density at 3.984 °C, a minimum in the isothermal compressibility at 46.5 °C, and an unusual variation in the diffusion coefficient with pressure. These trends are especially apparent in supercooled water where one can also find a minimum in both the density[11] and a dynamic transition to Arrhenius behavior for the diffusion coefficient.[12,13] It has been suggested that many of the anomalous properties of water at low temperatures could be understood by a hypothesized second critical point[14–16] buried deep within "no-man's land,"[17] a region of the phase diagram inaccessible to experiment. If this is so, it would go a long way to explaining another feature of water; its capacity to form several amorphous phases (glasses) at low temperatures.

In elucidating the origin of these anomalies, computer simulations have played a prominent role, for example, their part in the proposal of a second critical point in water[14,18] using a simple empirical model. Classical computer simulations do, however, have their limitations. There are certain systems, water being one of them, where quantum effects are significant.[19,20] As an example, let us examine the difference in temperature between the melting point and the temperature of maximum density. For H_2O this amounts to 3.984 K, whereas for D_2O it is 7.365 K. From the point of view of the Born–Oppenheimer approximation the potential energy surface (PES) is independent of the isotope considered. Thus the different behavior of these isotopes is due to how the molecules react to this PES. This is known as an atomic quantum delocalization effect. In this particular case the origin of the differences, both structural and dynamical, is in good part due to the quantum nature of the hydrogen protons and the strength of the hydrogen bond. Another example is the self-diffusion coefficient, which increases by more than 50% in a quantum system with respect to classical molecular dynamics simulations.[21,22]

The overall structure of water is that of an asymmetric top, which is to say that all three principal moments of inertia are distinct. What is particularly interesting is that since hydrogen is the lightest atom, the rotational moments of inertia are small enough to show the marked quantum behavior. Thus water has significant quantum effects even at room temperature. The importance of these quantum effects increases as the temperature is lowered. For the ice phases these effects are expected to be significant, especially at 77 K where many experiments on ice are frequently performed using liquid nitrogen. Thus far there has been relatively little work on these effects for ice and almost all of the work that

a)Electronic mail: cvega@quim.ucm.es.

has been published has focused on ice I_h.[21,23–25] The objective of this publication is to quantify the size of these effects in all of the ice phases, apart from that of ice X, which cannot be described by the rigid models used in this work.

These atomic quantum delocalization effects will be studied using the empirical TIP4P/2005 model.[26] Over the last few years a number of the present authors have undertaken extensive simulation studies examining the performance of a number of commonly used models for water, in particular, the TIP3P, TIP4P, TIP5P, and simple point charge/extended (SPC/E) models.[27] The principal findings have been that the TIP3P,[28] TIP5P,[29] and SPC/E (Ref. 30) models experience difficulties when it comes to describing the global phase diagram of water and the ice phases. However, the TIP4P model does indeed provide a qualitatively correct phase diagram. Based on this finding, the TIP4P model was reparametrized in order to improve the quantitative representation, leading to the TIP4P/2005 model.[31] It has since been found that this model also provides a good description of the maximum in density of liquid water and its variation with pressure[32] of the compressibility minima,[32] the surface tension,[33] the vapor liquid equilibria,[34] the critical properties,[34] the equation of state at high pressures,[27] the diffusion coefficient,[27] and the viscosity.[27]

That said, the model was parametrized for classical simulations, so the introduction of atomic quantum delocalization effects, although improving the qualitative description, will cause a deterioration in the quantitative description. In the first stage of this research we shall analyze the impact of atomic quantum delocalization effects on the properties of the ice phases using this potential. That will elucidate where and how atomic quantum delocalization effects modify the properties of water with respect to the classical limit. These differences then known, we provide a reparametrized version of the TIP4P/2005 model which we shall call the TIP4PQ/2005 model, the *Q* indicating that this model is suitable for quantum simulations. As was pointed out by Morse and Rice[35] as well as by Whalley,[36] "…effective potentials that are used to simulate water ought to be tested on the many phases of ice before being treated as serious representations of liquid water."

II. METHODOLOGY

Simulations were performed using the path integral formulation, which permits us to study the quantum effects related to the finite mass of the atoms (in many quantum chemistry calculations, the electrons are treated as being quantum; however the nuclei are treated as classical point masses). A particularly elegant technique for studying quantum effects in many body systems is that of path-integral Monte Carlo (PIMC). There are many good introductions concerning PIMC in the literature;[37–41] here we shall focus on the aspects most pertinent to the simulations we have performed.

Water is, of course, a flexible molecule. For path integral simulations one generally requires the number of Trotter slices P to be[42]

$$P > \frac{\hbar \omega_{\max}}{k_B T}, \tag{1}$$

where $\omega_{\max}$ is the "fastest" frequency present in the system in question. In water the intramolecular vibrations are of the order of $\omega_{\max}/2\pi c \approx 4000\ \mathrm{cm}^{-1}$ which leads to $P > 20$. Using the rigid body approximation for water the fastest motion now becomes the libration with a frequency of $<900\ \mathrm{cm}^{-1}$, thus reducing P to around 5 and 6. This represents a substantial reduction in the computational overhead associated with traditional PIMC calculations (although new techniques have recently been developed by Manolopoulos and co-workers[42] to increase the efficiency of flexible molecule PIMC). It must be said that by choosing to use a rigid model, one precludes the ability to study some aspects of water such as the high frequency region of the infrared adsorption spectrum.[43,44] The infrared spectrum of water and ice can be divided up into two distinct regions. Above $\approx 900\ \mathrm{cm}^{-1}$ one has the contribution associated with the intramolecular degrees of freedom of bending and stretching. Below $\approx 900\ \mathrm{cm}^{-1}$, as previously mentioned, one has the section that corresponds to translational and librational movements and are mostly due to intermolecular forces. Quantum contributions to the Helmholtz energy (A) within a perturbative treatment for a rigid asymmetric top are given by[45]

$$\frac{A - A_{C1}}{N} = \frac{\hbar^2}{24(k_B T)^2}\left[\frac{\langle F^2\rangle}{M} + \frac{\langle \Gamma_A^2\rangle}{I_A} + \frac{\langle \Gamma_B^2\rangle}{I_B} + \frac{\langle \Gamma_C^2\rangle}{I_C}\right] - \frac{\hbar^2}{24}\sum_{\text{cyclic}}\left(\frac{2}{I_A} - \frac{I_A}{I_B I_C}\right) + \mathcal{O}(\hbar^4). \tag{2}$$

A good proportion of the quantum effects in water are due to the strength of the hydrogen bond along with a particularly small inertia tensor. It is this that lends importance to the torque (Γ) terms found in the above equation, which results in the appearance of the librational band. In contrast, this region for a molecule such as SO_2, where no such hydrogen bonding is present, is far less important. By using the path integral formulation for a rigid model we shall be studying atomic quantum delocalization effects in the influential region encountered below $\approx 900\ \mathrm{cm}^{-1}$. In a study of the phonon density of states for ice I_h Dong and Li[46] showed that the rigid TIP4P model does a reasonable job of reproducing this low frequency section of the spectrum. Even given the fact that intramolecular effects are important, it is surely the case that a rigid body path-integral study is more physically realistic than a purely classical study, which neglects all atomic quantum delocalization effects. Such an approach has been adopted in a number of studies using, for example, the SPC/E model.[22] In view of this and given the success that the TIP4P/2005 model has had in describing the ice phases classically, the rigid TIP4P/2005 model is the natural candidate for a preliminary study of atomic quantum delocalization effects in ices. Given that the TIP4P/2005 model is a rigid asymmetric top, we shall first present the path integral description of a rigid rotor.

A. Path integrals for a rigid molecule

The coordinates used to describe a rigid molecule are $\mathbf{r}_1\boldsymbol{\Omega}_1$, where $\mathbf{r}_1$ represents the center of mass and $\boldsymbol{\Omega}_1=(\phi_1,\theta_1,\chi_1)$ represents the Euler angles that fix the molecule orientation. The Hamiltonian of a rigid asymmetric rotor can be written in the form[47]

$$\hat{H}_1=\hat{T}^{\mathrm{tra}}+\hat{T}^{\mathrm{rot}}+\hat{U}, \tag{3}$$

where $\hat{T}^{\mathrm{tra}}$ represents the kinetic energy operator associated with the center of mass translation, $\hat{U}$ appears as a potential energy operator that is a function of the coordinates $\mathbf{r}_1\boldsymbol{\Omega}_1$, and the rotational kinetic energy operator is given by[47]

$$\hat{T}^{\mathrm{rot}}=\sum_{i=1}^{3}\frac{\hat{L}_i^2}{2I_i}, \tag{4}$$

where $\hat{L}_i$ are the components of the angular momentum operator and I_i are the moments of inertia of the molecule referred to its fixed body frame. We assume, without loss of generality, that the moment of inertia tensor is diagonal in the chosen fixed body frame.

In the path integral formulation, the partition function Q_1 of a rigid molecule may be expressed by a factorization of the density matrix into P factors, so that each quantum particle is described by a ring of P replicas or "beads,"

$$Q_1(\beta)=\lim_{P\to\infty}\int\cdots\int\prod_{t=1}^{P}d\mathbf{r}_1^t d\boldsymbol{\Omega}_1^t\prod_{t=1}^{P}\rho_1^{t,t+1}(\beta/P), \tag{5}$$

where $\beta=1/k_BT$ is the inverse temperature and the propagator $\rho_1^{t,t+1}$ is approximated by[47]

$$\rho_1^{t,t+1}(\beta/P)\approx\langle\mathbf{r}_1^t\boldsymbol{\Omega}_1^t|\exp[-\beta\hat{U}/2P]\exp[-\beta(\hat{T}^{\mathrm{tra}}+\hat{T}^{\mathrm{rot}})/P]\times\exp[-\beta\hat{U}/2P]|\mathbf{r}_1^{t+1}\boldsymbol{\Omega}_1^{t+1}\rangle. \tag{6}$$

The propagator satisfies the cyclic condition that bead $P+1$ corresponds to bead 1. This rigid molecule propagator is built up of three factors: A potential energy component, a translational component, and a rotational component,

$$\rho_1^{t,t+1}(\beta/P)\approx\rho_{\mathrm{pot},1}^{t,t+1}\rho_{\mathrm{tra},1}^{t,t+1}\rho_{\mathrm{rot},1}^{t,t+1}. \tag{7}$$

The potential energy component is given by[47]

$$\rho_{\mathrm{pot},1}^{t,t+1}=\exp\left[-\frac{\beta}{2P}(U^t+U^{t+1})\right], \tag{8}$$

where $U^t=U(\mathbf{r}_1^t\boldsymbol{\Omega}_1^t)$ is the potential energy of the replica t of the molecule. The translational component is given by[47]

$$\rho_{\mathrm{tra},1}^{t,t+1}=\langle\mathbf{r}_1^t|\exp(-\beta\hat{T}^{\mathrm{tra}}/P)|\mathbf{r}_1^{t+1}\rangle=\left(\frac{MP}{2\pi\hbar^2\beta}\right)^{3/2}\exp\left[-\frac{MP}{2\hbar^2\beta}(\mathbf{r}_1^t-\mathbf{r}_1^{t+1})^2\right], \tag{9}$$

where M is the total mass of the rigid molecule. The two previous equations are well known and are commonly used as the so-called primitive approximation in path integral studies of simple fluids. The rotational propagator between t and $t+1$ is given by[47]

$$\rho_{\mathrm{rot},1}^{t,t+1}=\langle\boldsymbol{\Omega}_1^t|\exp[-\beta\hat{T}^{\mathrm{rot}}/P]|\boldsymbol{\Omega}_1^{t+1}\rangle. \tag{10}$$

In an important piece of work Müser and Berne[47,48] showed that the rotational contribution to the propagator between the replicas t and $t+1$ of a rigid molecule i is exactly given by

$$\rho_{\mathrm{rot},i}^{t,t+1}(\tilde{\theta}_i^{t,t+1},\tilde{\phi}_i^{t,t+1}+\tilde{\chi}_i^{t,t+1})=\sum_{J=0}^{\infty}\sum_{M=-J}^{J}\sum_{\tilde{K}=-J}^{J}f_{i,J,M,\tilde{K}}^{t,t+1}\exp\left(-\frac{\beta E_{\tilde{K}}^{JM}}{P}\right), \tag{11}$$

where

$$f_{i,J,M,\tilde{K}}^{t,t+1}=\frac{2J+1}{8\pi^2}d_{MM}^{J}(\tilde{\theta}_i^{t,t+1})\cos[M(\tilde{\phi}_i^{t,t+1}+\tilde{\chi}_i^{t,t+1})]|A_{\tilde{K}M}^{(JM)}|^2. \tag{12}$$

Here $d_{MM}^{J}(\tilde{\theta}_i^{t,t+1})$ are Wigner functions and $|A_{\tilde{K}M}^{(JM)}|$ are the coefficients of the expansion of the eigenstates of the asymmetric top in a basis formed by the eigenstates of the symmetric top. $E_{\tilde{K}}^{(JM)}$ are the eigenvalues of the energy of the asymmetric top. The quantum numbers J and M provide the values of the total angular momenta of the asymmetric top and the value of its z component in the laboratory frame. The number $\tilde{K}$ is not a true quantum number in the sense that it does not provide the value of any physical observable, but rather is an index used to label the $(2J+1)$ energy levels that are obtained for each value of J. The angles $\tilde{\theta}_i^{t,t+1}$, $\tilde{\phi}_i^{t,t+1}$, and $\tilde{\chi}_i^{t,t+1}$ are the Euler angles of the replica $t+1$ of molecule i expressed in the body frame fixed in the replica t of the same molecule i. Note that the rotational propagator depends solely on two variables: $\tilde{\theta}_i^{t,t+1}$ and $\tilde{\phi}_i^{t,t+1}+\tilde{\chi}_i^{t,t+1}$. Obviously to determine the value of the rotational propagator one must first determine the $(2J+1)$ energy levels of the asymmetric top for each value of J. This can be obtained from the $(2J+1)$ eigenvalues $E_{\tilde{K}}^{(JM)}$ of the matrix given in Ref. 49. The coefficients $|A_{\tilde{K}M}^{(JM)}|$ are the eigenvectors associated with these eigenvalues. It is computationally convenient to calculate the rotational propagator $\rho_{\mathrm{rot},i}^{t,t+1}(\tilde{\theta}_i^{t,t+1},\tilde{\phi}_i^{t,t+1}+\tilde{\chi}_i^{t,t+1})$ for a grid of values of the angles $\tilde{\theta}_i^{t,t+1}$ and $\tilde{\phi}_i^{t,t+1}+\tilde{\chi}_i^{t,t+1}$ for each value of β/P to be used and save these data prior to the simulations. The value of the rotational propagator for any given $\tilde{\theta}_i^{t,t+1}$ and $\tilde{\phi}_i^{t,t+1}+\tilde{\chi}_i^{t,t+1}$ can then be estimated using a linear interpolation algorithm from these tabulated data.

B. Path integrals for an ensemble of rigid molecules

Once the translational and rotational propagators are known for a rigid molecule one can calculate the partition function for a set of interacting molecules. Let us assume that we shall be using a pairwise potential u_{ij} such that the potential energy of the replica t of the system is

$$U^t=\sum_i\sum_{j>i}u_{ij}(\mathbf{r}_i^t,\mathbf{r}_j^t,\boldsymbol{\Omega}_i^t,\boldsymbol{\Omega}_j^t). \tag{13}$$

Now the canonical partition function Q_N of an ensemble of N molecules described with P beads is given by

$$Q_N(\beta) \approx \frac{1}{N!}\left(\frac{MP}{2\pi\beta\hbar^2}\right)^{3NP/2}\int\cdots\int\prod_{i=1}^{N}\prod_{t=1}^{P} d\mathbf{r}_i^t d\Omega_i^t \times \exp\left(-\frac{MP}{2\beta\hbar^2}\sum_{i=1}^{N}\sum_{t=1}^{P}(\mathbf{r}_i^t-\mathbf{r}_i^{t+1})^2-\frac{\beta}{P}\sum_{t=1}^{P}U^t\right) \times\prod_{i=1}^{N}\prod_{t=1}^{P}\rho_{\mathrm{rot},i}^{t,t+1}. \quad (14)$$

As can be seen in Eqs. (13) and (14), each replica t of molecule i interacts (a) with the molecules that have the same index t via the intermolecular potential u_{ij}, (b) with replicas $t-1$ and $t+1$ of the same molecule i via a harmonic potential whose coupling parameter depends on the mass of the molecules M and on the inverse temperature β, and (c) with replicas $t-1$ and $t+1$ of the same molecule through the terms $\rho_{\mathrm{rot},i}^{t-1,t}$ and $\rho_{\mathrm{rot},i}^{t,t+1}$ which incorporate the quantization of the rotation, which in turn depends on the relative orientation of replica t with respect to $t-1$ and $t+1$ with respect to t.

Let us define an energy U' as

$$U' = \frac{MP}{2\beta^2\hbar^2}\sum_{i=1}^{N}\sum_{t=1}^{P}(\mathbf{r}_i^t-\mathbf{r}_i^{t+1})^2+\frac{1}{P}\sum_{t=1}^{P}U^t \quad (15)$$

and the total orientational propagator P_{rot} as

$$P_{\mathrm{rot}} = \prod_{i=1}^{N}\prod_{t=1}^{P}\rho_{\mathrm{rot},i}^{t,t+1}. \quad (16)$$

Within a Monte Carlo simulation one generates a new configuration starting from a previous configuration. The probability of accepting this new configuration p_{accept} is given by

$$p_{\mathrm{accept}} = \min\left[1,\exp(-\beta(U'_{\mathrm{new}}-U'_{\mathrm{old}}))\frac{P_{\mathrm{rot}}^{\mathrm{new}}}{P_{\mathrm{rot}}^{\mathrm{old}}}\right]. \quad (17)$$

It is worthwhile making two observations about the orientational propagator between a pair of contiguous beads $\rho_{\mathrm{rot},i}^{t,t+1}$. First, it must be positive in order to be used in the Metropolis acceptance criteria, which is indeed the case. Second, the maximum in the orientational propagator is achieved when $\tilde{\theta}=0$ and $\tilde{\phi}+\tilde{\chi}=0$. It is found that at high enough temperature the propagator decays to zero relatively quickly as the values of $\tilde{\theta}$ and $\tilde{\phi}+\tilde{\chi}$ increase. The orientational propagator can also be expressed as an auxiliary energy by defining $u_{i,\mathrm{aux}}$ such that

$$u_{i,\mathrm{aux}}^{t,t+1} = -\frac{1}{\beta}\ln\rho_{\mathrm{rot},i}^{t,t+1}. \quad (18)$$

$u_{i,\mathrm{aux}}$ has a minimum at $\tilde{\theta}=0$ and $\tilde{\phi}+\tilde{\chi}=0$ and increases quickly as a function of the variables $\tilde{\theta}$ and $\tilde{\phi}+\tilde{\chi}$. P_{rot} can now be written as

$$P_{\mathrm{rot}} = \exp(-\beta U_{\mathrm{aux}}) = \exp\left(-\beta\sum_{i=1}^{N}\sum_{t=1}^{P}u_{i,\mathrm{aux}}^{t,t+1}\right). \quad (19)$$

Using this auxiliary energy the Metropolis criteria can be now written as

$$p_{\mathrm{accept}} = \min[1,\exp(-\beta((U'_{\mathrm{new}}+U_{\mathrm{aux,new}}) - (U'_{\mathrm{old}}+U_{\mathrm{aux,old}})))]. \quad (20)$$

This expression helps us to clarify the role of the orientational propagator; it can be viewed as a potential that forces two contiguous beads t and $t+1$ to adopt similar orientations (this corresponds to the minimum of the auxiliary potential) with an energetic penalty when they adopt different orientations. This is analogous to the role played by the harmonic springs connecting the center of masses of the molecules in Eq. (15).

The internal energy can now be calculated from

$$E = -\frac{1}{Q_N}\frac{\partial Q_N}{\partial\beta}. \quad (21)$$

It can be shown that substituting the value of the canonical partition function in this expression results in

$$E = K_{\mathrm{tra}} + K_{\mathrm{rot}} + U, \quad (22)$$

where

$$K_{\mathrm{tra}} = \frac{3NP}{2\beta} - \left\langle\frac{MP}{2\beta^2\hbar^2}\sum_{i=1}^{N}\sum_{t=1}^{P}(\mathbf{r}_i^t-\mathbf{r}_i^{t+1})^2\right\rangle,$$

$$K_{\mathrm{rot}} = \left\langle\frac{1}{P}\sum_{i=1}^{N}\sum_{t=1}^{P}\frac{\Sigma_{J=0}^{\infty}\Sigma_{M=-J}^{J}\Sigma_{\tilde{K}=-J}^{J}f_{i,J,M,\tilde{K}}^{t,t+1}\tilde{E}_{\tilde{K}}^{JM}\exp\left[-\frac{\beta}{P}\tilde{E}_{\tilde{K}}^{JM}\right]}{\rho_{\mathrm{rot},i}^{t,t+1}}\right\rangle,$$

$$U = \left\langle\frac{1}{P}\sum_{t=1}^{P}U^t\right\rangle. \quad (23)$$

As with the rotational propagator, the numerator of K_{rot} in Eq. (23) was calculated prior to the simulations for a grid of the variables $\tilde{\theta}$ and $\tilde{\phi}+\tilde{\chi}$ and subsequently saved in tabular form.

When performing simulations of solids it is more convenient to perform the simulations in the NpT ensemble. The partition function for the NpT ensemble can be calculated using

$$Q_{NpT} = A\int dV\exp(-\beta pV)Q_N, \quad (24)$$

where A is a constant with units of inverse volume that makes Q_{NpT} dimensionless. Its value affects the Helmholtz energy function but not the configurational properties.

C. Simulation details

In this work PIMC simulations are undertaken for the TIP4P/2005 model for 14 of the 15 known ice phases. One of the most important variables when it comes to path integral simulations is the number of Trotter slices or beads (P) employed. If $P=1$ then the simulation is classical. As $P\rightarrow\infty$ then the quantum simulation becomes exact. Given the isomorphism between Trotter slices and the number of component beads in a ring polymer,[38] one can easily see that the time required for a simulation scales with the number of

TABLE I. Parameters for both the TIP4P/2005 and the TIP4PQ/2005 models. The distance between the oxygen and hydrogen sites is d_{OH}. The angle, in degrees, formed by hydrogen, oxygen, and the other hydrogen atom is denoted by $\angle$H–O–H. The Lennard-Jones site is located on the oxygen with parameters σ and ϵ. The charge on the proton is q_H. The negative charge is placed in a point M at a distance d_{OM} from the oxygen along the H–O–H bisector.

Model	d_{OH} (Å)	$\angle$H–O–H	σ (Å)	ϵ/k_B (K)	q_H (e)	d_{OM} (Å)
TIP4P/2005	0.9572	104.52	3.1589	93.2	0.5564	0.1546
TIP4PQ/2005	0.9572	104.52	3.1589	93.2	0.5764	0.1546

Trotter slices used. For flexible models of water at 300 K a typical number of slices is about $P=24$.[50–52] However, if a rigid model is employed, the number of Trotter slices required can be reduced by about a factor of 5.[24,53] Previous studies for a rigid model of water at 300 K found that a value of $P=5$ provides a good convergence.[23,24] Thus in this work the number of Trotter slices times the temperature was maintained at $PT\approx 1500$. For the lowest considered temperature (77 K) this corresponds to 20 beads. When computing the asymmetric top eigenenergies and eigenvectors of water the OH distance and the H–O–H bond angle of the TIP4P/2005 model were used, which corresponds to the gas phase geometry of real water. The principal moments of inertia are computed using this geometry along with the masses of the hydrogen and oxygen atoms. Although the model has the negative charge on the site M, this site is massless and therefore it is only used to compute the potential energy of the system.

In this work two models of water are studied, the TIP4P/2005 model[26] and a reparametrization, which we shall call the TIP4PQ/2005 model to "compensate" for quantum effects. The parameters for both of these models are given in Table I. The only difference between these models is an increase in the charges on the hydrogen sites by $0.02e$ along with a corresponding increase in the charge on the site M. For both models the Lennard-Jones potential was truncated at 8.5 Å and long-range corrections were included. The TIP4P/2005 model has been designed to be used with Ewald summation,[54,55] which is a well known technique to treat the long-range electrostatic interactions. Ewald summation is more appropriate than the reaction field method when it comes to the simulation of solid phases. The real part of the Coulombic potential was truncated at 8.5 Å.

The configurational space of the quantum system was sampled using a Monte Carlo code with four distinct types of trial moves: The displacement of a single bead of one molecule, rotation of a single bead of one molecule, translation of a whole ring, and rotation of all of the replicas of one molecule. A Monte Carlo cycle is defined as N Monte Carlo moves, where the probability of attempting a translation or a rotation of a single bead is 30% each and the probability of attempting a translation of a whole ring or rotating all the replicas of a ring is 20% each. The maximum displacement or rotation in each type of movement was adjusted to obtain a 40% acceptance probability. When simulations were performed in the NpT ensemble, besides the N particle trial moves, one Monte Carlo cycle also includes an attempt to change the volume of the simulation box. The maximum volume change was adjusted so as to obtain a 30% acceptance probability. In general the simulations consisted of 30 000 Monte Carlo equilibration cycles followed by a further 100 000 cycles for the accumulation of run averages. The number of molecules used in each of the phases is given in Table II. For the proton disordered ice phases the positions

TABLE II. Results for the TIP4P/$2005_{(PI)}$ model for the systems studied along with a comparison with classical results for the same model. All energies are in units of kcal/mol and the densities are in g cm^{-3}. The errors (in kcal/mol) are $\mathcal{O}(0.003)$ in $K_{translational}$, $\mathcal{O}(0.02)$ in $K_{rotational}$, $\mathcal{O}(0.02)$ in U, $\mathcal{O}(0.04)$ in E, and $\mathcal{O}(0.002)$ g cm^{-3} in ρ.

Phase (N)	T (K)	p (bar)	$(3/2)RT$	$K_{translational}$	$K_{rotational}$	K_{total}	U	E	U (classical)	ρ (path integral)	ρ (classical)
I_h(432)	250	0	0.75	0.83	1.39	2.22	−12.38	−10.17	−13.35	0.899	0.920
I_c(216)	78	0	0.23	0.45	1.36	1.81	−13.03	−11.22	−14.58	0.906	0.943
II (432)	123	0	0.37	0.51	1.26	1.77	−12.83	−11.06	−14.07	1.160	1.198
III (324)	250	2800	0.75	0.83	1.35	2.18	−12.15	−9.96	−13.06	1.141	1.159
IV (432)	110	0	0.33	0.49	1.25	1.74	−12.44	−10.70	−13.74	1.248	1.292
V (504)	237.65	5300	0.71	0.80	1.35	2.14	−12.19	−10.04	−13.21	1.240	1.271
VI (360)	225	11 000	0.67	0.78	1.34	2.12	−12.21	−10.10	−13.11	1.356	1.379
VII (432)	300	100 000	0.89	1.05	1.44	2.49	−9.32	−6.83	−9.95	1.767	1.782
VIII (600)	77	24 000	0.23	0.49	1.17	1.76	−11.31	−9.65	−12.50	1.573	1.616
IX (324)	165	2800	0.49	0.63	1.33	1.96	−12.80	−10.84	−13.95	1.160	1.190
XI (360)	77	0	0.23	0.45	1.36	1.81	−13.04	−11.23	−14.60	0.906	0.945
XII (540)	260	5000	0.77	0.86	1.34	2.20	−11.97	−9.77	−12.85	1.267	1.296
XIII (504)	80	1	0.24	0.44	1.25	1.69	−12.76	−11.07	−14.16	1.217	1.261
XIV (540)	80	1	0.24	0.44	1.27	1.71	−12.80	−11.09	−14.25	1.280	1.331

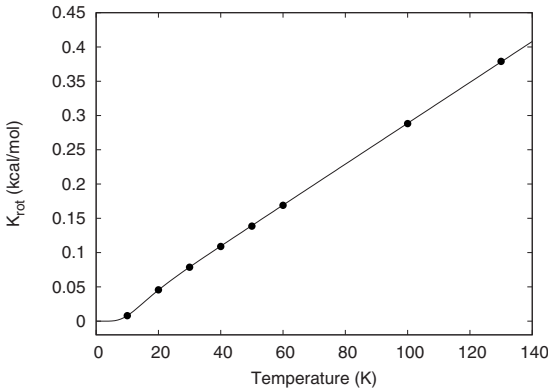

FIG. 1. Kinetic rotational energy from PIMC simulations of the isolated H_2O molecule (filled circles) as a function of temperature. Between 10 and 50 replicas (P) have been used depending on the temperature. There is a good agreement between the simulation data and the rotational energy obtained from the theoretical partition function of an asymmetric top having the H_2O geometry (solid line). The magnitude of the error is less than the size of the symbols shown.

of the hydrogen atoms were generated in such a way as to produce a system that satisfies the so-called Bernal–Fowler ice rules[56,57] and whose dipole moment as close as possible to zero. This was achieved using the algorithm proposed by Buch *et al.*[58,59]

As mentioned, all simulations were performed in the isothermal-isobaric (NpT) ensemble. The implementation of the NpT ensemble in PIMC has already been discussed in previous works.[60,61] It is important to note that the Monte Carlo volume moves should be performed anisotropically in order to allow the simulation box to "relax" and obtain the true equilibrium unit cell of the model under consideration. In other words, the pressure on the simulation box should be hydrostatic; the pressure tensor is diagonal and each of the elements along the diagonal has the same value. If this is not the case the system will suffer stresses and the structure and thermodynamic properties will not reach their equilibrium values. This is achieved using the technique proposed by Parrinello and Rahman[62–64] and extended to Monte Carlo by Yashonath and Rao.[65] Briefly, the shape of the simulation box is defined by a so-called H-matrix representing the Cartesian coordinates of the vectors defining the simulation box. Each of the individual components of the H-matrix is adjusted randomly, leading to changes in both the simulation box lengths and in the geometry.

As a preliminary check that the Müser and Berne propagator was implemented correctly the rotational energies were calculated for an isolated H_2O molecule. In Fig. 1 the rotational energies computed from the exact expression of the quantum partition function of an asymmetric top[66] (with the appropriate rotational constants) are compared to those obtained from PIMC simulations. As can be seen the agreement is excellent. It should be noted that the present calculations do not include exchange effects. However, these are only expected to be relevant at temperatures below those that we have studied in this work.

III. RESULTS

A single state point has been simulated for each of the solid phases of water with the exception of ice X, which cannot be described by a rigid model.[9,10] The results of these simulations are presented in Table II. By comparing the densities obtained from classical TIP4P/2005 simulations to path integral simulations of the TIP4P/2005 model, which henceforth we shall denote as TIP4P/$2005_{(PI)}$, it is clear that the introduction of atomic quantum delocalization effects reduces the density of the solid phase by about 0.02 g/cm^3 for temperatures above 200 K and by $\approx 0.03-0.04$ g/cm^3 for temperatures in the range of 75–170 K. Not surprisingly, quantum effects become increasingly evident as the temperature is reduced. The various contributions to the total energy E are also tabulated. As far as the translational kinetic energy component $K_{\text{translational}}$ is concerned one can observe an increase of about 10% for TIP4P/$2005_{(PI)}$ with respect to TIP4P/2005 [i.e., $(3/2)RT$] at temperatures above 225 K. As the temperature is lowered, this difference becomes 100%. This is approximately true for all of the ices. From these results one can conclude that the translational contribution to the heat capacity in quantum simulations is significantly less than the corresponding contribution in classical simulations. If one looks at the rotational kinetic energy contribution $K_{\text{rotational}}$, the differences are exaggerated even further; ranging from about 100% for "high" temperature ices and increasing to 600% at low temperatures. From this it is clear that the quantum contributions are manifestly rotational in their nature while translational effects are secondary in the solid phase. Within a perturbative treatment the quantum contribution to the Helmholtz energy function is related to the average of the forces divided by the masses for the translational contribution and to the average of the torques divided by the principal moments of inertia for the orientational contribution.[41] The mass of water is almost the same as that of neon; however, the quantum effects are far more pronounced in water for the temperature range considered in this work.[67] The overwhelming reason for this difference is the strength and directionality of the hydrogen bond. This, as well as the fact that the moments of the inertia tensor are quite small due to hydrogen having a very low mass. The temperature dependence of the kinetic rotational energy is rather weak, so its contribution to the heat capacity is expected to be small. On the other hand the quantum contributions to the potential energy are of the order of 1 kcal/mol at high temperatures, which increases to 1.5 kcal/mol at low temperatures. Thus there is a significant difference in E between the TIP4P/2005 and the TIP4P/$2005_{(PI)}$ results, amounting to about 3 kcal/mol at low temperatures, half of which being due to potential energy and the other half kinetic.

We shall now turn to the radial distribution functions. These histograms provide insights into the structure of a fluid on a molecular scale.[36,68] One of the first simulation studies of such functions for water using path integral simulations was undertaken by Rossky and co-workers[69–72] for the ST2 model. Given the low scattering factor of hydrogen, the oxygen-oxygen (g_{OO}) is the distribution function most accessible experimentally. Here we present the oxygen-oxygen radial distribution function for ices I_h, II, and VI (Figs. 2–4) for classical TIP4P/2005 and TIP4P/$2005_{(PI)}$. For ice I_h the experimental radial distribution function has also been plot-

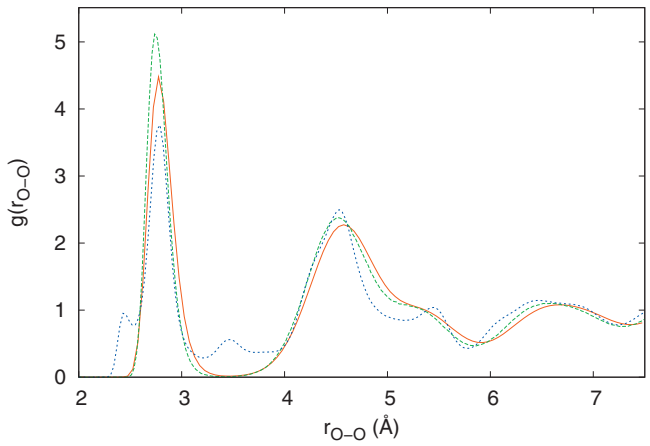

FIG. 2. Radial distribution function of ice I_h for TIP4P/2005 (dashed green line) and TIP4P/2005$_{(PI)}$ (solid red line) at 250 K and $p=0$ bar. The blue dotted line corresponds to the experimental data of Soper at 220 K (Ref. 73).

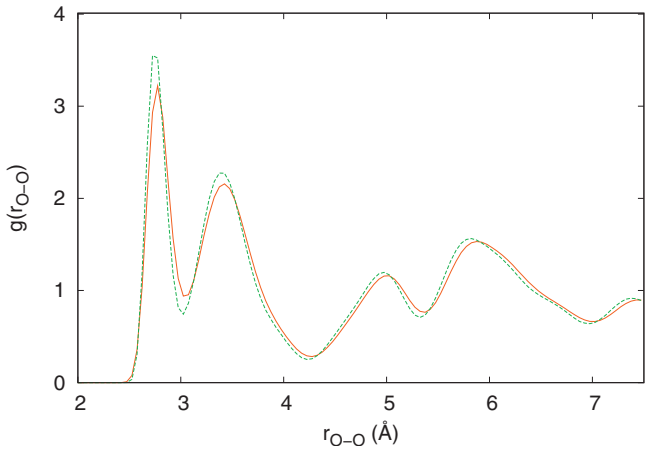

FIG. 4. Radial distribution function of ice VI for TIP4P/2005 (dashed green line) and TIP4P/2005$_{(PI)}$ (solid red line) at 225 K and $p=11$ kbar.

ted using the data provided by Soper[73] at 220 K. To the best of our knowledge as yet there are no experimental radial distribution functions available in the literature for ices II and VI. In Table III details are given for specific points located along the oxygen-oxygen radial distribution function curves for ice I_h. On going from classical simulations to path integral simulations the location of the first two peaks shifts to slightly larger distances. Furthermore, there is a notable reduction in the height of these peaks when quantum contributions are incorporated. Similar findings have been published previously for water and for simulations of TIP4P$_{(PI)}$ of ice I_h by de la Peña *et al.*[24] This softening of the distribution functions goes hand in hand with the reduction in the density of the ices in the PIMC calculations. It is interesting to speculate whether the addition of the small (and somewhat unusual) first peak in the ice I_h experimental data with the much larger second peak would place the simulation results in a more favorable light.

A consequence of the third law of thermodynamics is that the coefficient of thermal expansion α tends to zero when the temperature goes to zero. Experimentally one finds that there is very little variation in the density of ice I_h in the temperature range of 0–125 K. Classical simulations are unable to capture this, as can be seen in the low temperature equations of state published in Ref. 74, where the density of ice continues to increase as the temperature is lowered. Here we have performed simulations of TIP4P/2005$_{(PI)}$ for temperatures in the range of 77–200 K along the atmospheric pressure isobar for a number of ices. These results are presented in Table IV. In particular, the equation of state of ice I_h is plotted in Fig. 5 along with classical[74] and experimental results.[75] One can see a dramatic reduction in the density between classical TIP4P/2005 and TIP4P/2005$_{(PI)}$ simulations. However, the most important difference is that the density is almost independent of the temperature below $\approx$125 K; in other words, α tends to zero. Given the fact that the TIP4P/2005 model was parametrized for classical simulations, it is no surprise that the TIP4P/2005$_{(PI)}$ results show a significant deviation from the experimental values. That said, the TIP4P/2005$_{(PI)}$ curve is more or less parallel to the experimental curve, strongly suggesting that a reparametrization of the TIP4P/2005 model could improve these results by shifting the TIP4P/2005$_{(PI)}$ curve to higher densities. It is worth mentioning that the 100 K state point for the TIP4P/2005$_{(PI)}$ model seems to be slightly denser than the 77 K state point. It has been suggested that there is a temperature of maximum density in the ice phase;[76,77] however, longer and more detailed simulations would have to be undertaken to establish whether our results do indeed reflect this or not, given that this curvature could well be due to the statistical uncertainties in the simulation results.

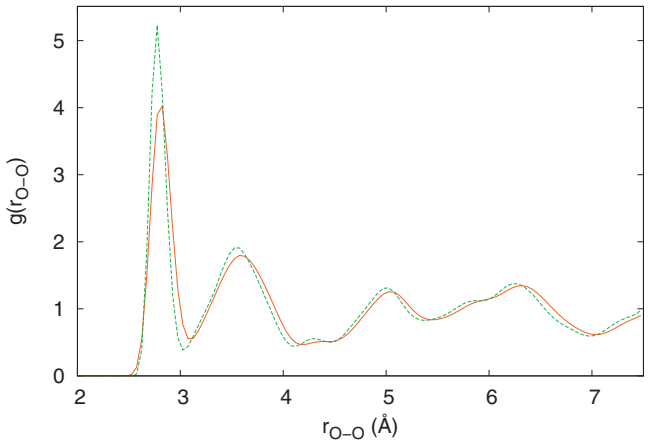

FIG. 3. Radial distribution function of ice II for TIP4P/2005 (dashed green line) and TIP4P/2005$_{(PI)}$ (solid red line) at 123 K and $p=0$ bar.

In 1984 Whalley[36] estimated the thermodynamic properties of ices at 0 K. This estimate was made after analyzing the experimental coexistence curves between ices at low temperatures and realizing that at 0 K phase transitions occur with zero enthalpy change. By assuming that the volume and internal energy difference between ices are largely unaffected by pressure (a quite reasonable approximation) Whalley was able to estimate the energies and densities of ices at 0 K and zero pressure. Such a calculation is useful as it allows one to obtain an idea of the form of the phase diagram at low temperatures by examining the relative stability of the ice phases. Thus one can estimate the coexistence pressure between two ice phases at 0 K using the approximation

TABLE III. Oxygen-oxygen radial distribution function of ice I_h for various water models at 250 K and $p=0$ bar.

	Peak 1		Peak 2		
Model	r (Å)	Height	r (Å)	Height	Ref.
TIP4P (classical)	2.725	4.707	4.525	2.279	68
TIP4P (path integral)	2.7625	4.167	4.5625	2.122	This work
TIP4P/2005 (classical)	2.7375	5.113	4.5125	2.382	This work
$TIP4P/2005_{(PI)}$	2.7875	4.481	4.5875	2.270	This work
TIP4PQ/2005	2.7625	4.725	4.5375	2.405	This work

$$p_{\mathrm{eq}} = \left. \frac{-\Delta U}{\Delta V} \right|_{p=0}. \tag{25}$$

More recently a similar analysis was undertaken[78] for a number of popular empirical models of water. For the SPC/E and TIP5P models ice II was found to be more stable than ice I_h; however, for TIP4P/2005 ice I_h, as is the experimental situation, was more stable than ice II. Here simulations were performed at 125, 100, and 77 K for $TIP4P/2005_{(PI)}$ (for technical reasons PIMC simulations at 0 K are infeasible, given the number of beads required). Assuming that the heat capacity C_p follows the Debye law, i.e., $C_p \propto T^3$, then it follows that the enthalpy should scale as T^4. Note that the internal energy and enthalpies are almost indistinguishable at room pressure; the pV term is negligible compared to the internal energy term. In Fig. 6 the internal energies from Table IV are plotted as a function of the temperature for $TIP4P/2005_{(PI)}$ and the estimated values at 0 K obtained from a fit of the form $E=a+bT^4$ are given in Table V. The relative energies between ices obtained at 0 K from the extrapolation procedure described above are quite similar to those obtained from the simulation results at 77 K. The inclusion of quantum effects consistently increases the energy at 0 K of the ice phases by ≈3.5 kcal/mol. However, for ices II, III, V, and VI the relative energy remains largely unchanged, differing by only ≈0.1 kcal/mol from the classical values. The zero point energies of ices II, III, V, and VI are quite similar and are expected to have a very little effect on the relative stability of the ice phases. This is not the case for ice I_h, atomic quantum delocalization effects destabilize ice I_h with respect to ice II, the difference now being

TABLE IV. Results for the $TIP4P/2005_{(PI)}$ model for the low temperature ice phases at a pressure of 1 bar. The energies are in units of kcal/mol and the densities are in g cm^{-3}. The errors (in kcal/mol) are $\mathcal{O}(0.003)$ in $K_{\mathrm{translational}}$, $\mathcal{O}(0.02)$ in $K_{\mathrm{rotational}}$, $\mathcal{O}(0.02)$ in U, $\mathcal{O}(0.04)$ in E, and $\mathcal{O}(0.002)$ g cm^{-3} in ρ.

Phase	T (K)	$K_{\mathrm{translational}}$	$K_{\mathrm{rotational}}$	K_{total}	U	E	ρ
I_h	200	0.70	1.36	2.06	−12.62	−10.56	0.903
I_h	150	0.58	1.35	1.93	−12.84	−10.91	0.906
I_h	125	0.53	1.35	1.87	−12.92	−11.05	0.907
I_h	100	0.48	1.35	1.83	−12.99	−11.15	0.907
I_h	77	0.45	1.36	1.80	−13.02	−11.22	0.906
II	200	0.69	1.28	1.96	−12.54	−10.57	1.145
II	150	0.57	1.25	1.82	−12.77	−10.95	1.155
II	125	0.51	1.24	1.75	−12.85	−11.09	1.159
II	100	0.47	1.24	1.71	−12.92	−11.21	1.163
II	77	0.43	1.26	1.84	−12.94	−11.26	1.165
III	200	0.70	1.32	2.02	−12.35	−10.34	1.106
III	150	0.58	1.29	1.87	−12.58	−10.70	1.116
III	125	0.53	1.30	1.82	−12.66	−10.84	1.122
III	100	0.48	1.30	1.77	−12.74	−10.96	1.125
III	77	0.44	1.30	1.74	−12.77	−11.02	1.130
V	200	0.69	1.30	1.99	−12.28	−10.29	1.204
V	150	0.57	1.28	1.85	−12.51	−10.67	1.217
V	125	0.52	1.28	1.78	−12.60	−10.81	1.222
V	100	0.47	1.28	1.74	−12.67	−10.92	1.225
V	77	0.44	1.28	1.72	−12.70	−10.99	1.227
VI	200	0.69	1.27	1.96	−12.19	−10.22	1.282
VI	150	0.58	1.25	1.83	−12.41	−10.58	1.296
VI	125	0.51	1.25	1.76	−12.50	−10.74	1.302
VI	100	0.46	1.25	1.71	−12.57	−10.86	1.306
VI	77	0.43	1.26	1.69	−12.60	−10.91	1.309

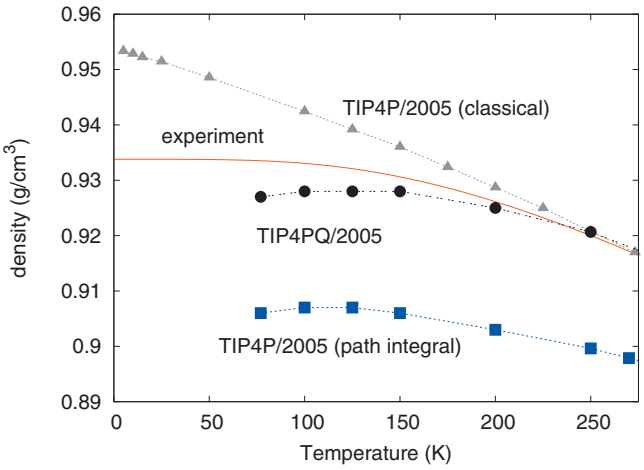

FIG. 5. Equations of state for ice I_h at $p=1$ bar. Classical TIP4P/2005 model (gray dot-dashed line/filled triangles) (Ref. 74), experimental data (red solid line) (Ref. 75), TIP4P/2005$_{(PI)}$ (blue dotted line/filled squares), and the new TIP4PQ/2005 model (black double-dotted line/filled circles). The error in the density is of order ± 0.002 g cm^{-3}.

TABLE V. Comparison of the energies E at 0 K for a selection of phases for both the TIP4P/2005$_{(PI)}$ and the TIP4PQ/2005 models as well as results for the classical TIP4P/2005 model (Ref. 78). The energies are in units of kcal/mol. The lowest energy (most stable phase) is shown in bold font. The lower section provides the relative energies with respect to ice II.

	E (0 K estimate)			
Ice	TIP4P/2005	TIP4P/2005$_{(PI)}$	TIP4PQ/2005	Expt.[a]
I_h	**−15.059**	−11.240	**−12.477**	**−11.315**
II	−14.847	**−11.290**	−12.436	−11.301
III	−14.741	−11.048	−12.210	−11.100
V	−14.644	−11.013	−12.152	−11.088
VI	−14.513	−10.939	−12.033	−10.928
I_h	**−0.212**	0.050	**−0.041**	**−0.014**
II	0	**0**	0	0
III	0.106	0.242	0.226	0.201
V	0.203	0.277	0.285	0.213
VI	0.334	0.351	0.403	0.373

[a]Reference 36.

≈0.26 kcal/mol. For example, for TIP4P/2005$_{(PI)}$ ice II replaces I_h as the most stable ice phase at low temperatures. Given the fact that quantum effects stabilize ice II with respect to ice I_h implies that for the TIP3P, SPC/E, and TIP5P models the inclusion of atomic quantum delocalization effects would further deteriorate their phase diagrams; the ice I_h phase being stable only for large negative pressures and ice II dominating the low temperate atmospheric pressure isobar. An interesting question is precisely why ice I_h is more affected than the rest of the ices by these atomic quantum delocalization effects. As discussed previously, within a perturbative treatment the effect of atomic quantum delocalization effects can be expressed as the average of forces and torques on the molecules divided by their masses or principal moments of inertia. Since the mass and inertia tensors are the same, regardless of the ice phase considered, differences between ices must be due to differences in forces and torques between molecules. In all the ices each water molecule forms four hydrogen bonds with its nearest neighbors. For ice I_h, the four nearest neighbors form an almost perfect tetrahedron. However, for ices II, III, V, and VI, the four nearest bonds form a distorted tetrahedron,[79] resulting in weaker hydrogen bonds (even though they are more dense than ice I_h). It is the strength of the I_h hydrogen bonding that is showing up in the quantum contributions.

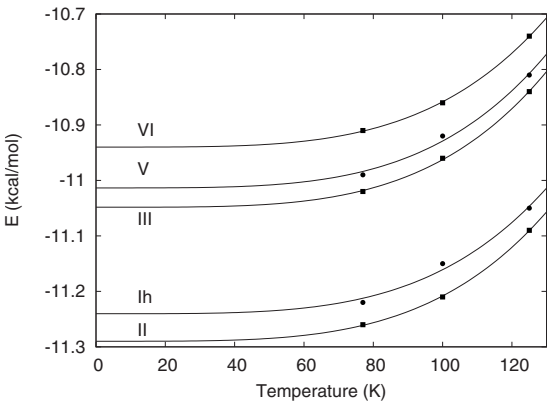

FIG. 6. Plot of the total energy of ices I_h, II, III, V, and VI at low temperatures for $p=1$ bar for TIP4P/2005$_{(PI)}$. Lines correspond to the fit $E=a+bT^4$. The error in the total energy is of order ± 0.04 kcal/mol.

The results presented thus far have elucidated the quantum contributions to the properties of the solid phases of water. The TIP4P/2005 model used in this study was originally parametrized to reproduce as faithfully as possible the experimental results for water using classical simulations. Thus in some implicit way, quantum contributions form part of the makeup of this model. It is no surprise that an explicit introduction of quantum effects will degrade the qualitative aspects of this model, which is exactly what we have seen in this work using TIP4P/2005$_{(PI)}$. We have witnessed that quantum effects decrease both the structure and the density of the ices as the temperature is lowered and that they modify the relative stability of ices I_h and II. Originally the TIP4P/2005 model was created by examining the derivatives of the parameters of the model for a number of properties, and then via a least-squares fit, the optimum values for the parameters are obtained. These properties include the density and the coexistence lines obtained from values of the Helmholtz energy function. However, here we do not yet have access to the coexistence lines for the TIP4P/2005$_{(PI)}$ model, so in developing the new TIP4PQ/2005 model, a modest and quite probably suboptimal change in the parameters was called for.

There is a veritable plethora of classical empirical models for water in the literature. In contrast, there is a paucity of quantum empirical models. It is worth making a mention of three of these quantum models: A reparametrization of a flexible version of the SPC/Fw model,[80] the second is a reparametrization of the rigid TIP5P model,[53] and the third is a series of flexible and polarizable potential models named TTM2-F[81] and TTM3-F,[82] obtained from fits to the potential energies of water clusters obtained from first principles calculations. For both the SPC and the TIP5P reparametrizations the essential difference was that the dipole moment of

TABLE VI. PIMC results for the TIP4PQ/2005 model for the systems studied and their relation to the experimental densities. All energies are in units of kcal/mol and the densities are in g cm^{-3}. The errors (in kcal/mol) are $\mathcal{O}(0.003)$ in $K_{\text{translational}}$, $\mathcal{O}(0.02)$ in $K_{\text{rotational}}$, $\mathcal{O}(0.02)$ in U, $\mathcal{O}(0.04)$ in E, and $\mathcal{O}(0.002)$ g cm^{-3} in ρ.

Phase	T (K)	p (bar)	$(3/2)RT$	$K_{\text{translational}}$	$K_{\text{rotational}}$	K_{total}	U	E	ρ (path integral)	ρ (Expt.)	Ref.
I_h	250	0	0.75	0.83	1.45	2.28	−13.74	−11.46	0.921	0.920	85
I_c	78	0	0.23	0.46	1.43	1.89	−14.33	−12.44	0.925	0.931	86
II	123	0	0.37	0.52	1.32	1.85	−14.06	−12.21	1.185	1.190	87
III	250	2800	0.75	0.84	1.41	2.25	−13.44	−11.18	1.159	1.165	88
IV	110	0	0.33	0.50	1.32	1.82	−13.63	−11.81	1.276	1.272	89
V	237.65	5300	0.71	0.81	1.41	2.22	−13.43	−11.21	1.266	1.271	90
VI	225	11 000	0.67	0.79	1.39	2.18	−13.41	−11.23	1.377	1.373	91
VII	300	100 000	0.89	1.05	1.47	2.52	−10.37	−7.85	1.780	1.880	92
VIII	77	24 000	0.23	0.50	1.23	1.73	−12.28	−10.56	1.592	1.628 (at 10 K)	91
IX	165	2800	0.49	0.64	1.39	2.04	−14.07	−12.03	1.182	1.194	88
XI	77	0	0.23	0.46	1.43	1.89	−14.34	−12.46	0.926	0.934 (at 5 K)	93
XII	260	5000	0.77	0.87	1.40	2.27	−13.23	−10.96	1.297	1.292	94
XIII	80	1	0.24	0.46	1.32	1.77	−13.95	−12.17	1.242	1.244	95
XIV	80	1	0.24	0.46	1.34	1.80	−13.99	−12.20	1.307	1.332	95

the molecule was increased while maintaining the remaining parameters of the potential constant. The basic idea is that since atomic quantum delocalization effects reduce the density and increase the internal energy of the system, increasing the charge is a simple way of "recompensating" for these changes, coaxing the model back to being its former self. It was with this in mind that the TIP4PQ/2005 model was created. The only difference between the TIP4P/2005 and the TIP4PQ/2005 models is in the dipole moment (see Table I), which was increased from 2.305 to 2.38 D. This was achieved by a $0.02e$ increase in the charge of the protons. Similar increases in the dipole moments of water (of about 0.08–0.10 D) were used in the aforementioned quantum versions of SPC (Ref. 80) and TIP5P models.[53] Such an increase in the charge may not be necessary in a flexible model where, as stated by Mahoney and Jorgensen,[53] "…although quantum effects make the density behavior of the rigid model worse, they improve the density behavior of the flexible model." This interplay between an increase in the dipole moment and flexibility has also been commented upon by other authors.[83,84] Obviously this new model is only suitable for quantum simulations of water.

In Table VI the state points for the ice phases are recalculated using this new TIP4PQ/2005 model. When compared to the experimental values[85–95] the results are really quite good over the whole range of temperatures and pressures. The average quadratic deviation between experimental and predicted densities (excluding ice VII) is 0.01 g/cm^3 for the classical TIP4P/2005 model, which becomes 0.03 g/cm^3 for the TIP4P/2005$_{(\text{PI})}$ model. For the reparametrized TIP4PQ/2005 model the quadratic deviation is once again 0.01 g/cm^3, recovering the situation for the classical model for the state points considered. In Table VII the unit cell parameters for the TIP4PQ/2005 model for a selection of ice phases have been provided and are also seen to be rather good when compared to the experimental values.

In Fig. 5 the equation of state for ice I_h is plotted. The TIP4PQ/2005 state points are equidistant from those of TIP4P/2005$_{(\text{PI})}$, but they are now much closer to the experimental values with a deviation of around 0.005 g/cm^3, which amounts to a difference of only 0.8% with respect to the experimental value. Given the curvature of the equation of state, in line with the third law of thermodynamics, and the small difference between the TIP4PQ/2005 densities and the experimental results leads us to believe that this is one of the best theoretical descriptions of ice I_h thus far seen in the literature. This is not to say that in the future this cannot be improved upon, for example, via the inclusion of flexibility, polarizability, etc. in the molecular model. In Fig. 7 the oxygen-oxygen radial distribution function of ice I_h at 77 K is compared to the experimental results of Narten *et al.*,[96] and the results are acceptable almost all the way up to 9 Å. The most notable difference can be seen in the height of the first peak, which drops from 9.37 for classical TIP4P/2005 down to 6.21 for TIP4PQ/2005, compared to 5.95 experimentally.[96]

In an analogous study to that for 0 K for TIP4P/2005$_{(\text{PI})}$ the relative stability of ices I_h, II, III, V, and VI at low temperatures has been tabulated in Tables V and VIII and plotted in Fig. 8. As can be seen the relative energy between ice II and the remainder of the ices is similar to that of

TABLE VII. Unit cell parameters for the TIP4PQ/2005 model for a selection of ice phases. Experimental values are from Table 11.2 of Ref. 2. Note that for ice II the hexagonal unit cell rather than the rhombohedral unit cell is given. All distances are in angstrom.

Phase	T (K)	p (bar)	Unit cell	
			Expt.	Simulation
I_h	250	0	a=4.518, c=7.356	a=4.483, c=7.352
II	123	0	a=12.97, c=6.25	a=12.98, c=6.23
III	250	2800	a=6.666, c=6.936	a=6.645, c=7.011
V	100	1	a=9.22, b=7.54, c=10.35, β=109.2°	a=9.06, b=7.64, c=10.21, β=108.6°
VI	225	11 000	a=6.181, c=5.698	a=6.167, c=5.713

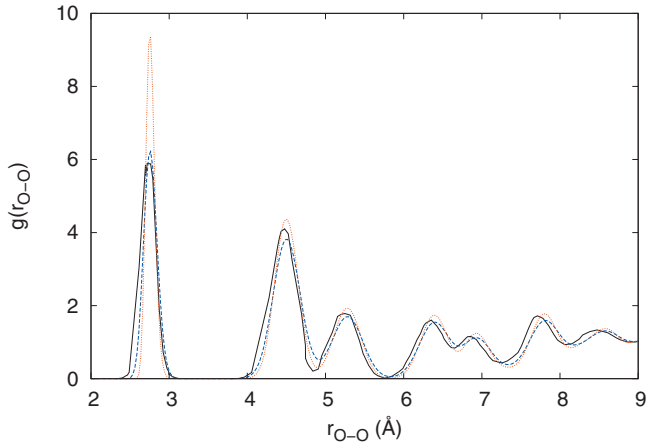

FIG. 7. Radial distribution function of ice I_h for the TIP4PQ/2005 model using PIMC (dashed blue line) compared to the classical TIP4P/2005 model (dotted red line) and with experimental data (solid red line) (Ref. 96) at 77 K and $p=1$ bar.

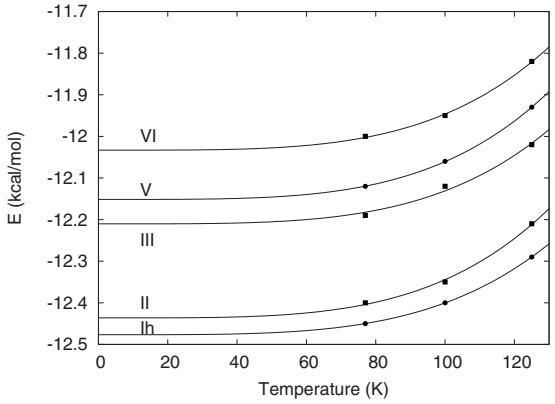

FIG. 8. Plot of the total energy of ices I_h, II, III, V, and VI at low temperatures for $p=1$ bar for the TIP4PQ/2005 model. Lines correspond to the fit $E=a+bT^4$. The error in the total energy is of order ± 0.04 kcal/mol.

TIP4P/2005$_{(PI)}$. The most significant result is that for TIP4PQ/2005 ice I_h regains its rightful place as the most stable ice phase. Experimentally the energy difference between I_h and II is 0.014 kcal/mol, which for TIP4PQ/2005 becomes 0.04 kcal/mol. In Table IX results for the 0 K coexistence pressures calculated using Eq. (25) are presented. It can be seen that both the energies (Table V) and the coexistence pressures (Table IX) for various transitions are substantially better than the values provided by classical simulations of the TIP4P/2005 model, in particular, for the I_h-II transition. This gives us confidence that the TIP4PQ/2005 could well produce a respectable global phase diagram in the future.

IV. CONCLUSIONS

This work addresses a series of physical properties of water that vary with the inclusion of atomic quantum delocalization effects, which were introduced to the TIP4P/2005 model using PIMC simulations. Quantum simulations have been undertaken for all of the ice phases of water with the exception of ice X, for the TIP4P/2005 model, and for the new TIP4PQ/2005 model. Using the Müser and Berne propagator for rigid asymmetric tops, various properties of these ices have been examined.

It has been found that the radial distribution functions become more "washed out" when quantum effects are taken into account. In other words, the peaks become lower and wider and shift to slightly larger distances. This goes hand in hand with a reduction in density for the quantum solid by ≈ 0.02 g/cm^3 for temperatures above 150 K and ≈ 0.04 g/cm^3 below 100 K.

If a classical empirical model is tailored to reproduce the experimental ice densities at a temperature close to the melting point, as the temperature is reduced the model will start to fail (such is the case, for example, of the TIP4P/2005

TABLE VIII. PIMC results for the TIP4PQ/2005 model for the low temperature ice phases at a pressure of 1 bar. All energies are in units of kcal/mol and the densities are in g cm^{-3}. The errors (in kcal/mol) are $\mathcal{O}(0.003)$ in $K_{\text{translational}}$, $\mathcal{O}(0.02)$ in $K_{\text{rotational}}$, $\mathcal{O}(0.02)$ in U, $\mathcal{O}(0.04)$ in E, and $\mathcal{O}(0.002)$ g cm^{-3} in ρ.

Phase	T (K)	$K_{\text{translational}}$	$K_{\text{rotational}}$	K_{total}	U	E	ρ
I_h	300	0.97	1.49	2.47	−13.46	−10.99	0.915
I_h	200	0.71	1.44	2.15	−13.98	−11.82	0.925
I_h	150	0.60	1.42	2.02	−14.18	−12.16	0.928
I_h	125	0.54	1.41	1.96	−14.25	−12.29	0.928
I_h	100	0.50	1.42	1.92	−14.32	−12.40	0.928
I_h	77	0.46	1.43	1.89	−14.34	−12.45	0.927
II	125	0.53	1.32	1.84	−14.06	−12.21	1.185
II	100	0.48	1.30	1.78	−14.14	−12.35	1.188
II	77	0.44	1.32	1.76	−14.16	−12.40	1.190
III	150	0.59	1.36	1.95	−13.83	−11.88	1.134
III	125	0.54	1.36	1.90	−13.92	−12.02	1.139
III	100	0.50	1.37	1.87	−13.98	−12.12	1.142
III	77	0.45	1.37	1.82	−14.01	−12.19	1.146
V	125	0.53	1.34	1.84	−13.80	−11.93	1.248
V	100	0.49	1.34	1.82	−13.88	−12.06	1.251
V	77	0.44	1.35	1.79	−13.91	−12.12	1.253
VI	125	0.53	1.32	1.85	−13.67	−11.82	1.330
VI	100	0.48	1.31	1.79	−13.74	−11.95	1.334
VI	77	0.45	1.32	1.77	−13.77	−12.00	1.336

TABLE IX. Estimates of the coexistence pressures (in bar) for the TIP4PQ/2005 model extrapolated to 0 K. Experimental values are taken from the work of Whalley (Ref. 36) and the values for the classical TIP4P/2005 model are from Ref. 78.

Phases	TIP4P/2005	TIP4PQ/2005	Expt. value
I_h-II	2090	400	140 ± 200
I_h-III	3630	3008	2400 ± 100
II-V	11 230	15 630	$18\,500 \pm 4000$
II-VI	8530	10 190	$10\,500 \pm 1000$
III-V	3060	1800	3000 ± 100
V-VI	6210	5580	6200 ± 200

model[74]). This is due to the fact that classical simulations are unable to satisfy one of the consequences of the third law of thermodynamics, namely, that the coefficient of thermal expansion α tends to zero as the temperatures approaches 0 K. It can be seen that the PIMC simulations now, to a good degree, correctly describe the low temperature physics of this model.

The translational component of the kinetic energy bears a passing resemblance to the classical value of $(3/2)RT$, whereas the rotational component is markedly larger. There is a particularly pronounced effect in the relative stabilities of ices I_h and II, where the stability of ice II is enhanced by the inclusion of atomic quantum delocalization effects.

In this work a reparametrization of the TIP4P/2005 model is provided that compensates for the quantum effects so as to maintain the quantitative performance of the TIP4P/2005 model, while at the same time reproducing the correct physics at low temperatures. In this new model, which we have called TIP4PQ/2005, the only parameter to have changed is that of the dipole moment; the charge on the hydrogen atom has been increased by $0.02e$, thus the dipole moment increases from 2.30 to 2.38 D.

In this paper it is shown that the TIP4PQ/2005 model provides a good description of the densities of the ice phases for the state points considered. The ice I_h $p=1$ bar isobar has been calculated and the tendency for α to become zero is now present in the equation of state. This new model also correctly describes the relative stabilities of ices I_h and II. An extrapolation indicates that at 0 K I_h is more stable than ice II by 0.04 kcal/mol (compared to 0.014 kcal/mol experimentally). The inclusion of quantum effects substantially improves the overall description of all of the ice phases studied here. The TIP4P/2005 does a reasonable job but the TIP4PQ/2005 is clearly superior. This paper can be regarded as a first step in introducing atomic quantum delocalization effects in the description of the solid phases of water. However, it is by no means the last word, since obviously water is a flexible molecule. In our opinion the results in the present manuscript could be very useful as a point of departure for the development of a flexible model of water for use in path integral simulations and provide valuable material from which to make comparisons. Such comparison would establish just how much of the quantum effects in water are due to intra and how much is due to the intermolecular degrees of freedom.

ACKNOWLEDGMENTS

The authors would like to thank J. L. Abascal for insightful conversations and M. I. J. Probert for his hospitality and illuminating discussions while one of the authors, C.V., was in York. We would also like to thank the reviewers for their useful comments regarding the manuscript. This work has been funded by DGI (Spain) (Grant Nos. FIS2007-66079-C02-01 and FIS2006-12117-C04-03), by the Comunidad Autonoma de Madrid (Grant No. S-0505/ESP/0299) (MOSSNOHO), and by the Universidad Complutense de Madrid (Grant No. 910570). E.G.N. would like to thank the MEC for a Juan de la Cierva fellowship.

[1] D. Eisenberg and W. Kauzmann, *The Structure and Properties of Water* (Oxford University Press, New York, 1969).
[2] V. F. Petrenko and R. W. Whitworth, *Physics of Ice* (Oxford University Press, New York, 1999).
[3] F. Franks, *Water: A Matrix of Life*, 2nd ed. (RSC Publishing, London, 2000).
[4] P. Ball, *Life's Matrix: A Biography of Water* (University of California Press, Berkeley, 2001).
[5] P. Jungwirth, Faraday Discuss. **141**, 9 (2009).
[6] E. Sanz, C. Vega, J. L. F. Abascal, and L. G. MacDowell, Phys. Rev. Lett. **92**, 255701 (2004).
[7] A. F. Goncharov, N. Goldman, L. E. Fried, J. C. Crowhurst, I.-F. W. Kuo, C. J. Mundy, and J. M. Zaug, Phys. Rev. Lett. **94**, 125508 (2005).
[8] E. Schwegler, M. Sharma, F. Gygi, and G. Galli, Proc. Natl. Acad. Sci. U.S.A. **105**, 14779 (2008).
[9] M. Benoit, D. Marx, and M. Parrinello, Nature (London) **392**, 258 (1998).
[10] P. Loubeyre, R. LeToullec, E. Wolanin, M. Hanfland, and D. Hausermann, Nature (London) **397**, 503 (1999).
[11] D. Liu, Y. Zhang, C.-C. Chen, C.-Y. Mou, P. H. Poole, and S.-H. Chen, Proc. Natl. Acad. Sci. U.S.A. **104**, 9570 (2007).
[12] L. Xu, P. Kumar, S. V. Buldyrev, S.-H. Chen, P. H. Poole, F. Sciortino, and H. E. Stanley, Proc. Natl. Acad. Sci. U.S.A. **102**, 16558 (2005).
[13] P. Kumar, S. V. Buldyrev, S. R. Becker, P. H. Poole, F. W. Starr, and H. E. Stanley, Proc. Natl. Acad. Sci. U.S.A. **104**, 9575 (2007).
[14] P. H. Poole, F. Sciortino, U. Essmann, and H. E. Stanley, Nature (London) **360**, 324 (1992).
[15] P. G. Debenedetti and H. E. Stanley, Phys. Today **56**, 40 (2003).
[16] P. G. Debenedetti, J. Phys.: Condens. Matter **15**, R1669 (2003).
[17] H. E. Stanley, S. V. Buldyrev, M. Canpolat, O. Mishima, M. R. Sadr-Lahijany, A. Scala, and F. W. Starr, Phys. Chem. Chem. Phys. **2**, 1551 (2000).
[18] H. E. Stanley, C. A. Angell, U. Essmann, M. Hemmati, P. H. Poole, and F. Sciortino, Physica A **205**, 122 (1994).
[19] J. A. Morrone and R. Car, Phys. Rev. Lett. **101**, 017801 (2008).
[20] F. Paesani and G. A. Voth, J. Phys. Chem. B **113**, 5702 (2009).
[21] L. H. de la Peña and P. G. Kusalik, J. Chem. Phys. **125**, 054512 (2006).
[22] T. F. Miller and D. E. Manolopoulos, J. Chem. Phys. **123**, 154504 (2005).
[23] H. Gai, G. K. Schenter, and B. C. Garrett, J. Chem. Phys. **104**, 680 (1996).
[24] L. Hernandez de la Peña, M. S. Gulam Razul, and P. G. Kusalik, J. Chem. Phys. **123**, 144506 (2005).
[25] F. Paesani and G. A. Voth, J. Phys. Chem. C **112**, 324 (2008).
[26] J. L. F. Abascal and C. Vega, J. Chem. Phys. **123**, 234505 (2005).
[27] C. Vega, J. L. F. Abascal, M. M. Conde, and J. L. Aragones, Faraday Discuss. **141**, 251 (2009).
[28] W. L. Jorgensen, J. Chandrasekhar, J. D. Madura, R. W. Impey, and M. L. Klein, J. Chem. Phys. **79**, 926 (1983).
[29] M. W. Mahoney and W. L. Jorgensen, J. Chem. Phys. **112**, 8910 (2000).
[30] H. J. C. Berendsen, J. R. Grigera, and T. P. Straatsma, J. Phys. Chem. **91**, 6269 (1987).
[31] J. L. F. Abascal, E. Sanz, and C. Vega, Phys. Chem. Chem. Phys. **11**, 556 (2009).
[32] H. L. Pi, J. L. Aragones, C. Vega, E. G. Noya, J. L. F. Abascal, M. A. Gonzalez, and C. McBride, Mol. Phys. **107**, 365 (2009).
[33] C. Vega and E. de Miguel, J. Chem. Phys. **126**, 154707 (2007).

[34] C. Vega, J. L. F. Abascal, and I. Nezbeda, J. Chem. Phys. **125**, 034503 (2006).
[35] M. D. Morse and S. A. Rice, J. Chem. Phys. **76**, 650 (1982).
[36] E. Whalley, J. Chem. Phys. **81**, 4087 (1984).
[37] R. P. Feynman and A. R. Hibbs, *Path-Integrals and Quantum Mechanics* (McGraw-Hill, New York, 1965).
[38] D. Chandler and P. G. Wolynes, J. Chem. Phys. **74**, 4078 (1981).
[39] M. J. Gillan, *The Path-Integral Simulation of Quantum Systems*, NATO ASI Series C Vol. 293 (Kluwer, Dordrecht, 1990), Chap. 6, pp. 155–188.
[40] D. M. Ceperley, Rev. Mod. Phys. **67**, 279 (1995).
[41] M. P. Allen and D. J. Tildesley, *Computer Simulation of Liquids* (Oxford University Press, New York, 1987), Chap. 10.
[42] T. E. Markland and D. E. Manolopoulos, J. Chem. Phys. **129**, 024105 (2008).
[43] J. A. Poulsen, G. Nyman, and P. J. Rossky, Proc. Natl. Acad. Sci. U.S.A. **102**, 6709 (2005).
[44] S. Habershon, G. S. Fanourgakis, and D. E. Manolopoulos, J. Chem. Phys. **129**, 074501 (2008).
[45] J. G. Powles and G. Rickayzen, Mol. Phys. **38**, 1875 (1979).
[46] S. Dong and J. Li, Physica B **276–278**, 469 (2000).
[47] D. Marx and M. H. Müser, J. Phys.: Condens. Matter **11**, R117 (1999).
[48] M. H. Müser and B. J. Berne, Phys. Rev. Lett. **77**, 2638 (1996).
[49] R. N. Zare, *Angular Momentum: Understanding Spatial Aspects in Chemistry and Physics* (Wiley, New York, 1988).
[50] J. Lobaugh and G. A. Voth, J. Chem. Phys. **106**, 2400 (1997).
[51] H. A. Stern and B. J. Berne, J. Chem. Phys. **115**, 7622 (2001).
[52] W. Shinoda and M. Shiga, Phys. Rev. E **71**, 041204 (2005).
[53] M. W. Mahoney and W. L. Jorgensen, J. Chem. Phys. **115**, 10758 (2001).
[54] S. W. de Leeuw, J. W. Perram, and E. R. Smith, Proc. R. Soc. London, Ser. A **373**, 27 (1980).
[55] S. W. de Leeuw, J. W. Perram, and E. R. Smith, Proc. R. Soc. London, Ser. A **373**, 57 (1980).
[56] J. D. Bernal and R. H. Fowler, J. Chem. Phys. **1**, 515 (1933).
[57] L. Pauling, J. Am. Chem. Soc. **57**, 2680 (1935).
[58] V. Buch, P. Sandler, and J. Sadlej, J. Phys. Chem. B **102**, 8641 (1998).
[59] L. G. MacDowell, E. Sanz, C. Vega, and J. L. F. Abascal, J. Chem. Phys. **121**, 10145 (2004).
[60] J.-L. Barrat, P. Loubeyre, and M. L. Klein, J. Chem. Phys. **90**, 5644 (1989).
[61] M. H. Müser, P. Nielaba, and K. Binder, Phys. Rev. B **51**, 2723 (1995).
[62] M. Parrinello and A. Rahman, Phys. Rev. Lett. **45**, 1196 (1980).
[63] M. Parrinello and A. Rahman, J. Chem. Phys. **76**, 2662 (1982).
[64] R. Najafabadi and S. Yip, Scr. Metall. **17**, 1199 (1983).
[65] S. Yashonath and C. N. R. Rao, Mol. Phys. **54**, 245 (1985).
[66] I. N. Levine, *Molecular Spectroscopy* (Wiley, New York, 1975).
[67] R. Ramirez and C. P. Herrero, J. Chem. Phys. **129**, 204502 (2008).
[68] C. Vega, C. McBride, E. Sanz, and J. L. F. Abascal, Phys. Chem. Chem. Phys. **7**, 1450 (2005).
[69] R. A. Kuharski and P. J. Rossky, Chem. Phys. Lett. **103**, 357 (1984).
[70] R. A. Kuharski and P. J. Rossky, J. Chem. Phys. **82**, 5164 (1985).
[71] G. S. Del Buono, P. J. Rossky, and J. Schnitker, J. Chem. Phys. **95**, 3728 (1991).
[72] R. A. Kuharski and P. J. Rossky, J. Chem. Phys. **82**, 5289 (1985).
[73] A. K. Soper, Chem. Phys. **258**, 121 (2000).
[74] E. G. Noya, C. Menduiña, J. L. Aragones, and C. Vega, J. Phys. Chem. C **111**, 15877 (2007).
[75] R. Feistel and W. Wagner, J. Phys. Chem. Ref. Data **35**, 1021 (2006).
[76] H. Tanaka, J. Chem. Phys. **108**, 4887 (1998).
[77] Y. Koyama, H. Tanaka, G. Gao, and X. C. Zeng, J. Chem. Phys. **121**, 7926 (2004).
[78] J. L. Aragones, E. G. Noya, J. L. F. Abascal, and C. Vega, J. Chem. Phys. **127**, 154518 (2007).
[79] http://www.lsbu.ac.uk/water/.
[80] F. Paesani, W. Zhang, D. A. Case, T. E. Cheatham III, and G. A. Voth, J. Chem. Phys. **125**, 184507 (2006).
[81] C. J. Burnham and S. S. Xantheas, J. Chem. Phys. **116**, 5115 (2002).
[82] G. S. Fanourgakis and S. S. Xantheas, J. Chem. Phys. **128**, 074506 (2008).
[83] I. G. Tironi, R. M. Brunne, and W. F. van Gunsteren, Chem. Phys. Lett. **250**, 19 (1996).
[84] B. Guillot, J. Mol. Liq. **101**, 219 (2002).
[85] K. Röttger, A. Endriss, J. Ihringer, S. Doyle, and W. F. Kuhs, Acta Crystallogr., Sect. B: Struct. Sci. **50**, 644 (1994).
[86] W. F. Kuhs, D. V. Bliss, and J. L. Finney, J. Phys. Colloq. **48**, C1 (1987).
[87] A. D. Fortes, I. G. Wood, M. Alfredsson, L. Vocadlo, and K. S. Knight, J. Appl. Crystallogr. **38**, 612 (2005).
[88] J. D. Londono, W. F. Kuhs, and J. L. Finney, J. Chem. Phys. **98**, 4878 (1993).
[89] H. Engelhardt and B. Kamb, J. Chem. Phys. **75**, 5887 (1981).
[90] R. E. Gagnon, H. Kiefte, M. J. Clouter, and E. Whalley, J. Chem. Phys. **92**, 1909 (1990).
[91] W. F. Kuhs, J. L. Finney, C. Vettier, and D. V. Bliss, J. Chem. Phys. **81**, 3612 (1984).
[92] R. J. Hemley, A. P. Jephcoat, H. K. Mao, C. S. Zha, L. W. Finger, and D. E. Cox, Nature (London) **330**, 737 (1987).
[93] C. M. B. Line and R. W. Whitworth, J. Chem. Phys. **104**, 10008 (1996).
[94] C. Lobban, J. L. Finney, and W. F. Kuhs, Nature (London) **391**, 268 (1998).
[95] C. G. Salzmann, P. G. Radaelli, A. Hallbrucker, E. Mayer, and J. L. Finney, Science **311**, 1758 (2006).
[96] A. H. Narten, C. G. Venkatesh, and S. A. Rice, J. Chem. Phys. **64**, 1106 (1976).